

Small Structural Differences Between Two Ferrocenyl Diphenols Determine Large Discrepancies Of Reactivity And Biological Effects

Federica Tonolo,^[a] Michèle Salmain,^[b] Valeria Scalcon,^[a] Siden Top,^[b] Pascal Pigeon,^[b,c] Alessandra Folda,^[a] Benoit Caron,^[d] Michael J. McGlinchey,^[e] Robert-Alain Toillon,^[f] Alberto Bindoli,^[g] Gérard Jaouen,^[b,c] Anne Vessières,^{[b]*} and Maria Pia Rigobello^{[a]*}

[a] Dipartimento di Scienze Biomediche, Università di Padova, Via Ugo Bassi 58/b, 35131 Padova, Italy.

[b] Sorbonne Université, CNRS, IPCM, 4 Place Jussieu, 75005 Paris, France.

[c] Chimie ParisTech, PSL University, 11 rue Pierre et Marie Curie, 75005 Paris, France

[d] Sorbonne Université, IStEP, ALIPP6, 4 Place Jussieu, 75005 Paris, France

[e] School of Chemistry, University College Dublin, Belfield, Dublin 4, Ireland

[f] Université de Lille, INSERM U908, 59650 Villeneuve d'Ascq, France

[g] Istituto di Neuroscienze (CNR) Sezione di Padova, c/o Dipartimento di Scienze Biomediche, Via Ugo Bassi 58/b, 35131 Padova, Italy.

* To whom correspondence should be sent

A. Vessières: anne.vessieres@sorbonne-universite.fr

M.P. Rigobello: mariapia.rigobello@unipd.it

ID:	Title:	ORCID:
F. Tonolo	Dr.	0000-0002-7780-8994
M. Salmain	Dr.	0000-0003-3039-5659
V. Scalcon	Dr. PhD.	0000-0002-7061-6471
S. Top	Dr.	0000-0001-9068-4503
P. Pigeon	Dr.	0000-0001-5374-5346
A. Folda	Dr.	
B. Caron	Dr.	0000-0001-7051-4339
M.J. McGlinchey	Prof.	0000-0002-4342-0166
R.A. Toillon	Prof.	0000-0001-5483-2118
A. Bindoli	Dr.	
G. Jaouen	Prof.	0000-0001-5471-113X
A. Vessières	Dr.	0000-0002-4044-2730
M.P. Rigobello	Prof.	0000-0003-2586-3251

Abstract: Ferrocenyl diphenol complexes **1**, [1,1-bis(4'-hydroxyphenyl)-2-ferrocenyl-but-1-ene], and **Z-2**, [1,2-bis(4'-hydroxyphenyl)-1-ferrocenyl-but-1-ene], differing by the relative position of the two phenolic substituents, display dramatically different antiproliferative activities on cancer cells (**1** being by far more cytotoxic than **2**). In this paper our goal is to decipher the origin of this difference by comparing their reactivity and biological behaviour. In terms of common behaviour we found that **1** and **2** are both very efficient inhibitors of thioredoxin reductase (TrxR) *in vitro* after oxidation by the HRP/H₂O₂ system. However, as **1** is only a moderate inhibitor of TrxR in MDA-MB-231 cells, TrxR is probably not a major target responsible for the cytotoxicity of **1**. In terms of difference we noted that **1** induces a significant redox imbalance characterized by lipid peroxidation and thiol oxidation and a moderate decrease of the mitochondrial membrane potential in breast cancer cells while **2** has almost no effect. These results underline the importance of the *trans* configuration in the ferrocenyl /double bond / phenol motif, which is present in **1** but not in **Z-2** that exists only in a *cis* configuration.

Introduction

Metallodrugs based on the coordination chemistry of platinum, such as cisplatin, carboplatin and oxaliplatin, are used alone or in combination in over 50% of cancer treatments.¹⁻³ It is nevertheless well recognised that despite their proven capabilities, these entities have serious issues, including a general toxicity linked to their lack of selectivity between healthy and damaged cells, a fairly narrow therapeutic range, and a tendency to give rise to resistance problems.¹ This has led to research into other metallodrugs using different metals as well as different types of bonding such as those found in organometallic chemistry and characterised by covalent metal-carbon (M-C) bonds.^{2, 4, 5} The development of bioorganometallic chemistry with its novel functionalities has provided access to innovative properties that make it possible to reach different biological targets.⁴⁻⁷ In this context we have developed species incorporating ferrocene onto the tamoxifen skeleton, thus providing a new angle from which to view the question of what

antitumoral agents can do (proteic targets, selectivity for cancerous cells, avoidance of resistance effects, multiple mechanisms).⁸⁻¹² This family of complexes, known as ferrocifens, share a redox motif “ferrocenyl / alkene / phenol” generating as primary metabolites organometallic quinone methides (QM) whose electrophilicity can be modulated by ringing the changes among the substituents.^{8, 13-16} They are proving, both chemically and biologically, to be a very rich resource.^{9-12, 17}

In the ferrocifen family, the diphenolic complex **1** (Figure 1) was one of the first to be synthesized and studied. It was initially designed to shed light on the role of the dimethylaminopropyl substituent in **3** on its cytotoxic activity towards the hormone-independent breast cancer cell line MDA-MB-231.^{18, 19} Fortuitously, the cytotoxic activities of **1** and **3** were found very close ($IC_{50} = 0.6$ and $0.5 \mu\text{M}$ respectively on MDA-MB-231 cells), which makes them hits among this family of compounds which also includes the ansa-ferrociphenol complex **5**.^{10, 20} Complex **1**, formulated in lipid nano capsules (LNCs), was also the first in the family to show an antitumoral effect *in vivo* on rats with ectopic or orthotopic implanted tumours from glioblastoma (rat 9L cells).^{10, 11, 21} However, limited cell biology studies on **1** were performed only on glioma and melanoma cell lines.^{22, 23}

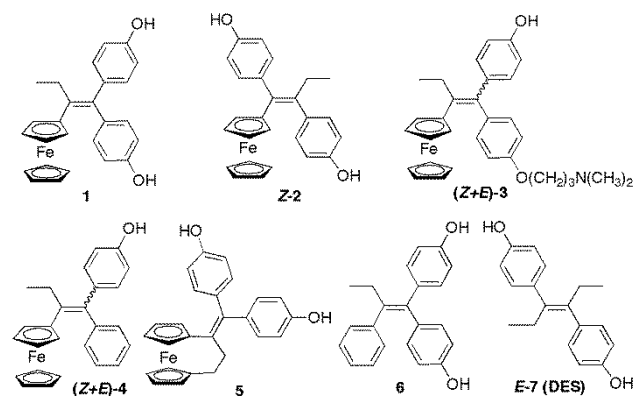


Figure 1. Structures of the ferrocenyl complexes and their corresponding organic molecules.

Subsequently, the ferrocenyl diphenol **2**, a regioisomer of **1** differing in the position of the two phenolic substituents on the carbons of the central double bond, was synthesized but its cytotoxicity was unexpectedly found to be much lower than that of **1**.^{24, 25} Recent results on **4**, the monophenol ferrocenyl complex, suggested that the mechanism of action of phenolic ferrocifens might differ from that of the tamoxifen-like complex **3**.²⁶ This difference was associated with the presence on **3** of the dimethylaminopropyl side chain. Recently, the QM of **3** was found to show a strong inhibitory activity on the enzyme thioredoxin reductase.²⁶ TrxR belongs to the thioredoxin system, which, together with the glutathione system, is responsible for thiol redox balance. TrxR displays a selenocysteine residue at its C-terminal active site, which acts as a major target of electrophiles as well as many metal complexes.²⁶⁻³⁰ TrxR is often overexpressed in many cancer cell lines and its inhibition brings to cell death.^{26, 28-30} We here report the results of a set of experiments on **1** and **2** carried out in an attempt to rationalize

their difference in cytotoxicity and also to give clues concerning their possible mechanism of action. For this purpose, two breast cancer cell lines, a hormone dependent (MCF-7) and a triple negative, hormone-independent (MDA-MB-231) were employed.

Results

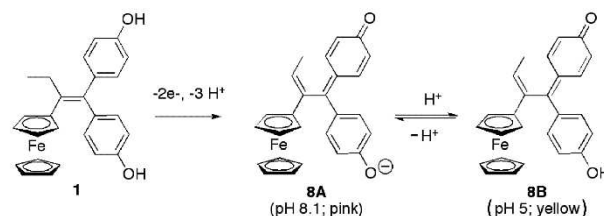
Syntheses of **1** and **2** were accomplished via the McMurry cross-coupling reaction of ketones according to a procedure previously described in the literature.^{19, 24, 25} Interestingly, complex **2** is obtained mainly as the *Z*-isomer (*Z/E* 93/7) whereby the two phenol groups are *trans* disposed. In addition, it was found that **Z-2** does not isomerize significantly even after one week in DMSO (*Z/E* = 99/1).²⁴ Complex **2** is the organometallic analogue of **E-7** (DES, diethylstilbestrol), and also exhibits a slow isomerisation.³¹ The almost exclusive formation of **Z-2**, and its resistance to isomerization, is rationalizable in terms of the steric problems engendered by positioning the two phenol moieties face to face in **E-2**. Preferential formation of **Z-2** in the McMurry reaction is determined by the transition state for radical coupling in which steric factors are minimized.³²

Enzymatic oxidation studies of **1**, **2** and the organic molecules **6** and **7** with the HRP/H₂O₂ system

Enzymatic oxidation reactions were performed with a 4-fold molar excess of H₂O₂ in the presence of horseradish peroxidase (HRP) at pH 8.1 or 5.0 and were monitored by UV-Vis spectroscopy.

Enzymatic oxidation of **1** and **6**

For **1**, a bright pink adduct ($\lambda_{\text{max}} = 565 \text{ nm}$) was formed very rapidly at pH 8.1 (Figure 2, upper panel) while the same experiment performed at pH 5 afforded a yellow adduct ($\lambda_{\text{max}} = 416 \text{ nm}$) (Figure S1 upper panel). When the experiment was performed at pH 6.8, we observed the presence of the two bands (Figure S1 lower panel). This behaviour is reminiscent of that previously observed for the ansa-ferrociphenol derivative **5**,³³ which lets us conclude that enzymatic oxidation of **1** affords the corresponding quinone methide in the anionic phenolate form **8A** at pH 8.1 or in the neutral phenolic form **8B** at pH 5.0 (Scheme 1) and the mixture of **8A** and **8B** at the intermediate pH 6.8.



Scheme 1. Proposed enzymatic oxidation sequence of **1** by the mixture HRP/H₂O₂.

The rate of formation of the QM of **1** at pH 8.1 was much faster than that of compound **5** (rate constant $k = 2.5 \text{ min}^{-1}$ for **1**, Figure S2 vs. 0.12 min^{-1} for **5** at pH 8)³³; its half-life is 12 min, and no intermediate was observed by UV-Vis spectroscopy. These differences may be explained in terms of the ring strain inherent in the ansa structure of **5**. Complex **8B** had been prepared previously by chemical oxidation with Ag_2O and characterized by NMR,³⁴ but cannot be obtained in the solid state due to its lowered stability compared to that of the quinone methide of **4** that can be isolated.²⁶

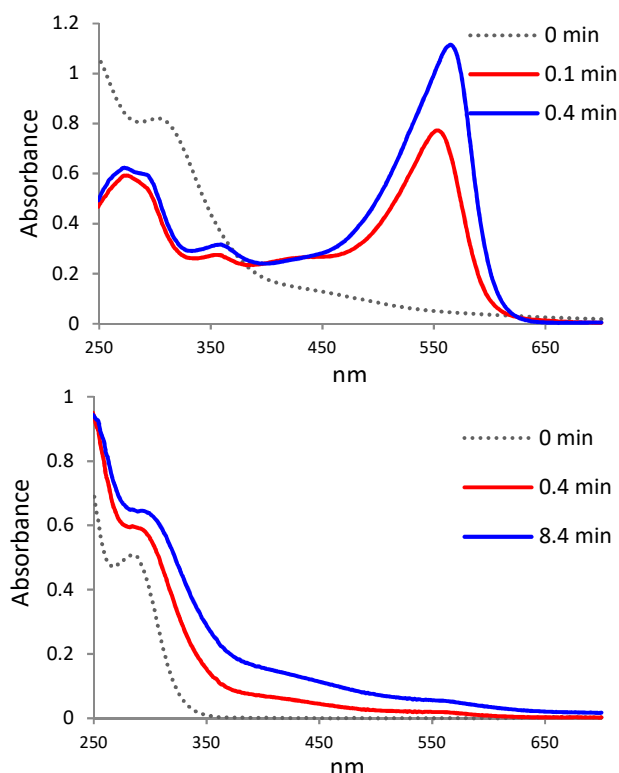


Figure 2. Time evolution of the UV-Vis spectrum of **1** (upper panel) and **6** (lower panel), $50 \mu\text{M}$, at 25°C in the presence of HRP (46 nM) and H_2O_2 ($200 \mu\text{M}$) at pH 8.1 (0.2 M Tris-HCl, 1 mM EDTA) containing 10% DMSO. Upper panel: pure **1** (0 min), band at 304 nm; after 0.1 min: bands at 553 nm (very intense), 358 nm (weak), 279 nm (broad, medium); after 0.4 min: bands at 565 nm (intense), 358 nm (weak) and 279 nm (broad, medium). Lower panel: Pure **6** (0 min) band at 284 nm; after 0.4 and 8.4 min: shoulder at 296 nm.

Complex **1** is the organometallic analogue of **6**, and interestingly, its treatment, in the same conditions, afforded non-identified compounds at both pH 8.1 (Figure 2 lower panel) and pH 5.0 (Figure S3) and in any case, not the quinone methide, indicating that the presence of the redox-active ferrocenyl unit on complex **1** was essential to drive quinone methide formation under oxidative conditions.

Enzymatic oxidation of **2** and **7**

Enzymatic oxidation of **2** at pH 8.1 led to the immediate formation of a blue-green adduct ($\lambda_{\text{max}} = 302, 408$ and 675 nm) followed by its conversion into another greenish product ($\lambda_{\text{max}} = 393$ and 629 nm) (Figure 3 upper panel).

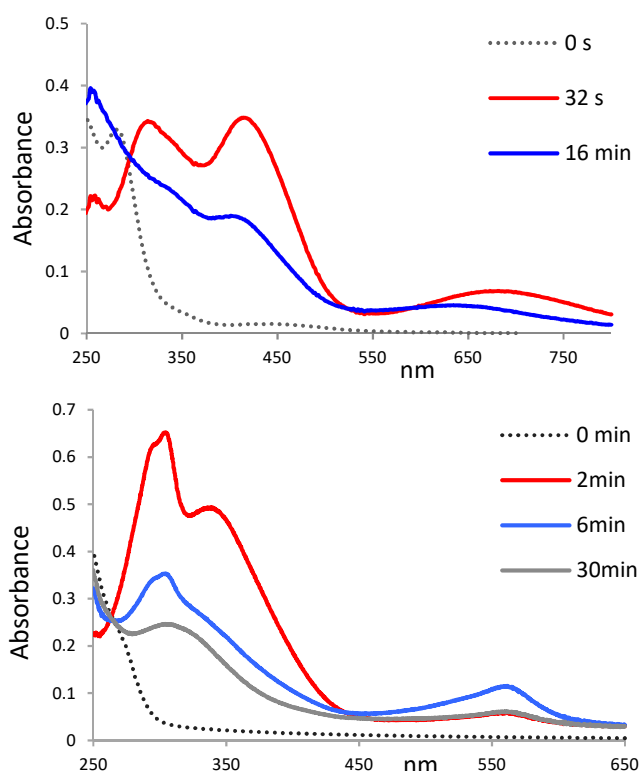
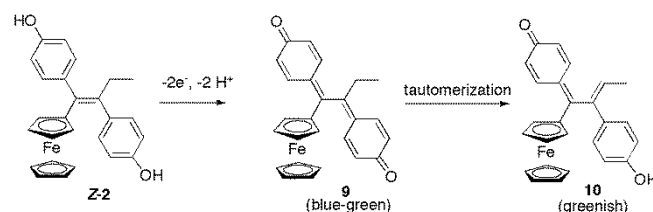


Figure 3. Time evolution of the UV-Vis spectrum of **2** (upper panel) and **7** (lower panel), $50 \mu\text{M}$, at 25°C in the presence of HRP (46 nM) and H_2O_2 ($200 \mu\text{M}$) at pH 8.1 (0.2 M Tris-HCl, 1 mM EDTA) containing 10% DMSO. Upper panel: pure **2** (0 min): band at 284 nm; after 32 s: bands at 683 nm (broad and weak), 416 and 316 nm (intense); after 16 min: bands at 638 nm (broad and weak), 408 (intense). Lower panel: pure **7** (0 min) no characteristic bands; after 2 min: bands at 304 and 338 nm (intense); after 6 min: bands at 306 nm (intense) and 561 nm (broad and weak), after 30 min these 2 bands have dramatically decreased.

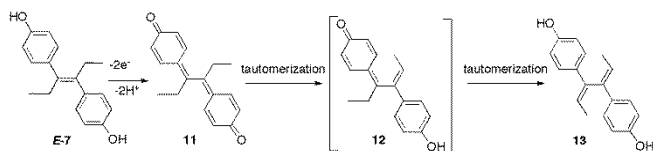
The colour of the first species is reminiscent of that of a ferrocenium species, which, according to the previously established mechanism of oxidation of ferrocifens, is the very first intermediate to be formed in the sequence of reactions leading to quinone methide (Scheme S1).¹⁷ However, an EPR (Electron Paramagnetic Resonance) experiment run on the mixture of **2** and H_2O_2 /HRP at very short incubation time invalidated this hypothesis since no signal corresponding to an iron-centred radical was detected. Indeed, chemical oxidation of **2** by Ag_2O was previously found to afford the phenol quinone compound **10** resulting from the loss of two electrons and two protons (Scheme 2).²⁴ This species was characterized by various spectroscopic techniques including its UV-Vis spectrum that displayed two characteristic bands at 392 and 590 nm in acetonitrile.



Scheme 2. Oxidation sequence of **2** involving loss of 2 electrons and 2 protons leading to **9**, the diquinone methide, then by tautomerization to the phenol-QM **10**.²⁴

The mechanism of oxidation of **2** to **10** is a two-step process whereby the diphenol compound is first rapidly converted into the diquinone **9** that undergoes subsequent tautomerization to afford **10**, the phenol-quinone.

For comparison the well-known estrogenic molecule **7** was enzymatically oxidized in the same way and the UV-Vis spectrum of the mixture was recorded over a period of 30 min (Figure 3, lower panel). Bands at 304 and 338 nm appeared within 2 min, and were readily assigned to the diquinone derivative **11** (Scheme 3). The system gradually evolved toward another species absorbing at 306 and 560 nm. It has been reported that **11** undergoes successive tautomerizations from **12** to **13** by migration of protons from the two ethyl substituents to afford the diphenol (Scheme 3).³⁵ The rate of conversion between **12** and **13** increased with the pH.³⁵ Compound **12**, the product of monotautomerization of **11**, the phenol-quinone, which is analogous to **10** the final oxidation product of complex **2**, has never been isolated. This second tautomerization is possible for **12** but not for **10**.



Scheme 3. Oxidation sequence of **E-7** involving loss of 2 electrons and 2 protons leading to **11**, the diquinone methide, then by a double tautomerization to the diphenol **13**.³⁵

Study of inhibition of cytosolic TrxR by **1** and **2**

To compare **1** and **2** with other ferrocenyl complexes, the potential effects on TrxR were investigated. Therefore, their inhibition on the isolated and purified cytosolic isoform of thioredoxin reductase (TrxR1) was measured. In accordance with previous results,^{28, 36} we tested the action of **1** and **2** alone or the compounds obtained by enzymatic oxidation by the HRP/H₂O₂ mixture of **1** and **2**, namely **8A** and **10**. As shown in

Figure 4, **1** and **2** determined only moderate inhibition of cytosolic TrxR1 (IC₅₀ = 19.36 μM and 32.2 μM, respectively), while **8A** and **10** were strong TrxR1 inhibitors (IC₅₀ = 27 nM and 31 nM, respectively). These values were lower than those found previously for **3** (IC₅₀ = 60 nM).²⁸ No inhibition of glutathione reductase (GR) by **1**, **2**, **8A**, and **10** was detected under similar conditions (Figure S4).

Mechanism of inhibition of TrxR1 by **1** and **2**

The BIAM (biotin-conjugated iodoacetamide) assay was used in order to gain information on the residues involved in the inhibition of TrxR1 induced by **1**, **2**, **8A** and **10**.

This assay evaluates the ability of the complexes to interact with the thiol and/or selenol groups borne by the cysteine and selenocysteine (Sec) residues of the enzyme. Actually, BIAM alkylates thiol and/or selenol groups depending on the pH. At pH 6.0, only selenocysteine and low pK_a cysteine were alkylated, while at pH 8.5, both selenocysteine and accessible cysteine were derivatized by BIAM. As shown in Figure 5, and in agreement with the TrxR1 inhibition pattern reported in Figure 4, both **8A** and **10** prevented the alkylation of TrxR1 by BIAM at pH 6 (**8A** being a little more efficient than **10**), indicating that both compounds were able to interact with the selenol group. At pH 8.5, full inhibition of BIAM alkylation by **8A** and **10** occurred, indicating that they were also able to interact with accessible cysteines. On the contrary, compounds **1** and **2** alone were scarcely effective. This type of result has been found previously for the ansa-ferrocenyl phenol derivative **5**,³³ while only derivatization of Sec was observed with **3**.²⁶

Antiproliferative activity of **1** and **2** on breast cancer cells

The antiproliferative activity of **1** and **2** was measured on two breast cancer cells (MDA-MB-231 and MCF-7) after 72 h by MTT cell viability assay. Complex **1** exhibited a high antiproliferative activity on both cancer cells lines (IC₅₀ = 0.98 and 0.7 μM, respectively), while complex **2** was markedly less cytotoxic (IC₅₀ = 69.8 and 25.5 μM, respectively). This result confirmed the low cytotoxicity previously found for **2**.^{24, 25}

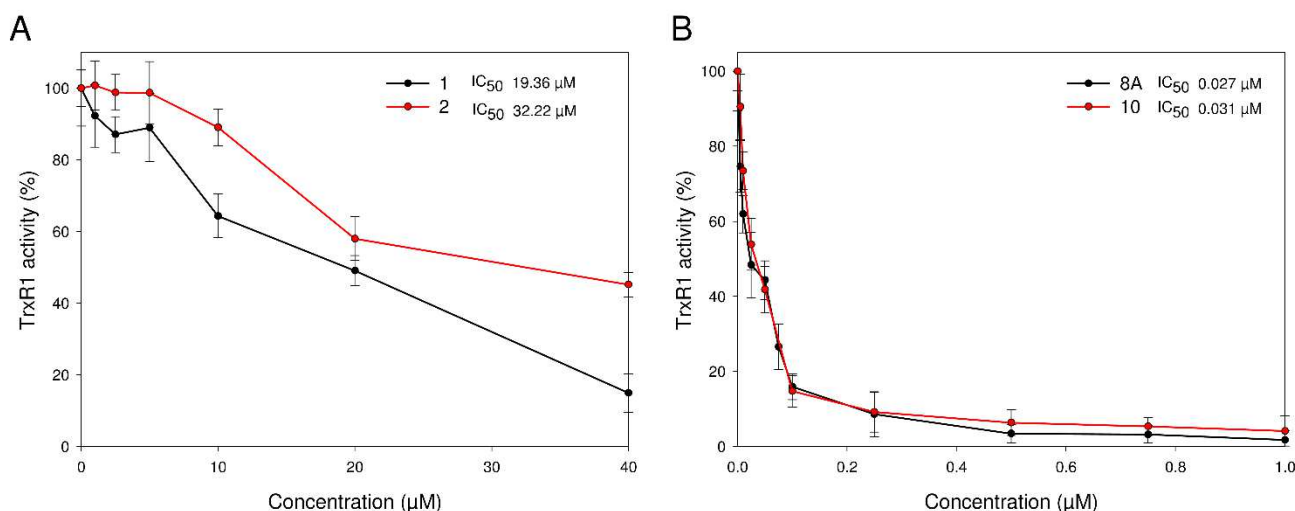


Figure 4. Concentration-dependent effects of **1**, **2** and **8A**, **10** (obtained after oxidation of **1** and **2** by the HRP/H₂O₂ mixture for 15 min) on the cytosolic thioredoxin reductase activity (see Experimental Section for details).

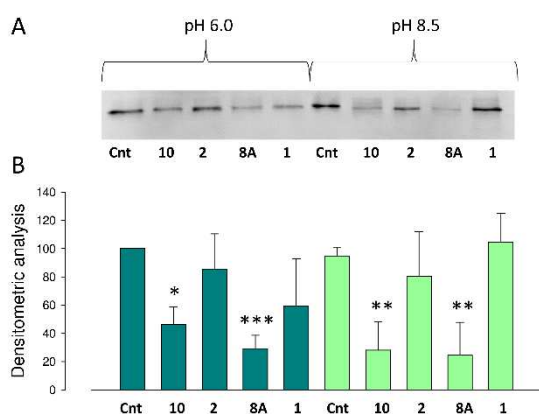
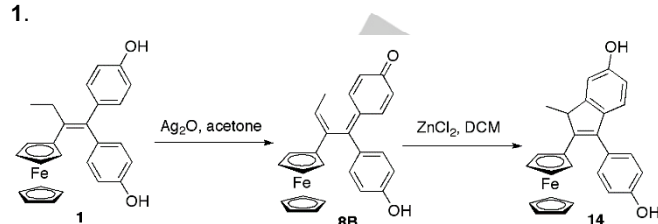


Figure 5. (A) BIAM assay of TrxR1 treated with **1**, **8A**, **2** and **10**. The complexes and their derivatives were incubated in the presence of a pre-reduced aliquot of TrxR1, as reported in the Experimental Section. Then, aliquots of the reaction mixture were added to 50 mM biotinylated iodoacetamide (BIAM) in buffer at either pH 6.0 (0.1 M HEPES-Tris) or pH 8.5 (0.1 M Tris-HCl) to alkylate the –SH/–SeH remaining groups. (B) Densitometric analysis was performed using Image J software. (* $p < 0.05$; ** $p < 0.01$; *** $p < 0.001$)

Inhibition of TrxR and GR induced by **1** and **2** in breast cancer cells

We next decided to evaluate the inhibitory effects of **1** and **2** on TrxR and GR activity in breast cancer cells. The enzymatic activity was measured in cell lysates, after incubation of cells with **1** or **2** at 20 or 40 μM for 18 h (Figure 6). Complex **1** induced a moderate inhibition of TrxR (around 25%) on MDA-MB-231 cells, but no inhibition on MCF-7 cells while **2** has almost no effect on both cell lines (Figure 6A). Regarding GR activity, **1** and **2** were almost ineffective, at both concentrations, on the two cell lines (Figure 6B). We also found that, under similar conditions (15 μM , 18h), **1** had no inhibitory effect on TrxR activity in Jurkat cells (Figure S5). Such a different behaviour towards TrxR in cancer cells and *in vitro* on purified enzyme has been previously observed for the monophenol complex **4**.²⁶ It was rationalized by the further conversion of its quinone methide into an indene in protic solvent. Indeed, indene **14** is readily obtained by treating **1** with Ag_2O as oxidant, followed by ZnCl_2 as Lewis acid (Scheme 4). In addition, it was also identified as one of the metabolites during the microsomal oxidation of **1**.³⁷ In contrast to the quinone methide, the indene

cannot undergo Michael additions, which may explain the limited inhibition of TrxR by **1** in cancer cells. This result suggests that inhibition of TrxR does not play a major role in the cytotoxicity of **1**.



Scheme 4. Formation of the indene **14** from compound **1**.³⁷

Quantification of total thiols in cancer cells incubated with **1** or **2**

Intracellular sulphhydryl groups are present in thiol/thiolates or disulphide forms depending on the redox state of cells. In addition to protein thiols, the most abundant low molecular weight thiol molecule in cells is glutathione, present at millimolar concentration. To investigate the action of **1** and **2** on the cellular redox balance, a quantification of total thiols in cells treated with 40 μM of **1** or **2** for 18 h was performed, and the results are shown in Table 1.

Table 1. Quantification of total thiols in control cells and cells incubated with **1** or **2** (40 μM , 18 h).

Compound	Total thiols (nmol / mg protein)	
	MDA-MB-231	MCF-7
None	38.2 \pm 7.8	48.9 \pm 7.9
1	21.3 \pm 0.6	40.2 \pm 5.1
2	40.6 \pm 5.1	46.1 \pm 7.8

These results showed that **1** induced a strong redox imbalance in MDA-MB-231 cells (44% decrease of thiol content) and a less pronounced action in MCF-7 cells (18% decrease of thiol) while **2** has almost no effect.

Evaluation of the mitochondrial membrane potential in cancer cells treated with **1** or **2**

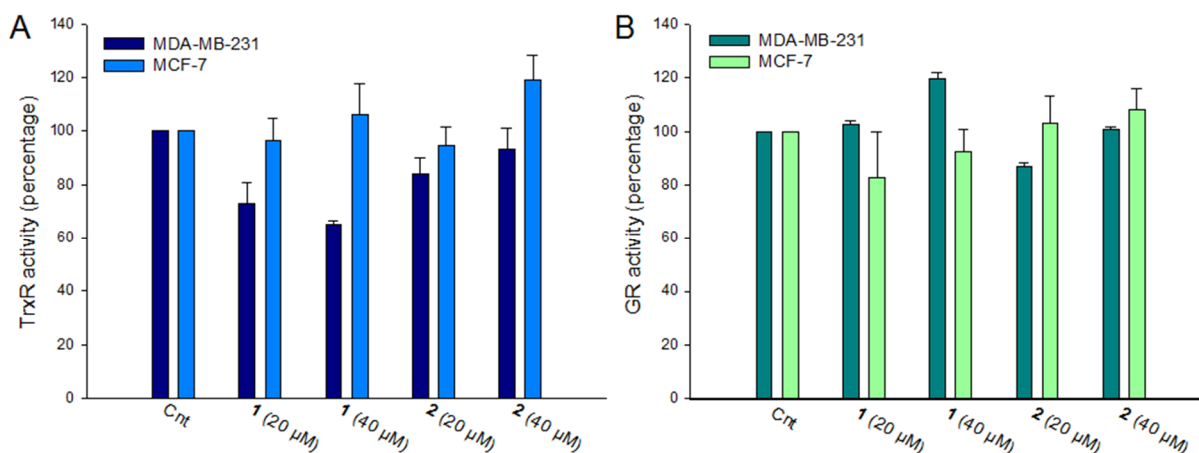


Figure 6. Effect of **1** and **2** on TrxR (A) and GR (B) enzymatic activities on MDA-MB-231 and MCF-7 cells.

The mitochondrial membrane potential (MMP) was evaluated on MDA-MB-231 and MCF-7 cells by flow cytometry using the fluorescent dye TMRM. As shown in Figure 7, complex **1** induced a significant decrease of MMP on both MDA-MB-231 and MCF-7 cells (30% of cells with low MMP after 18 h in the presence of 40 μM of **1**) while complex **2** was scarcely effective. A different behaviour was observed on Jurkat cells, where **1** had no effect.

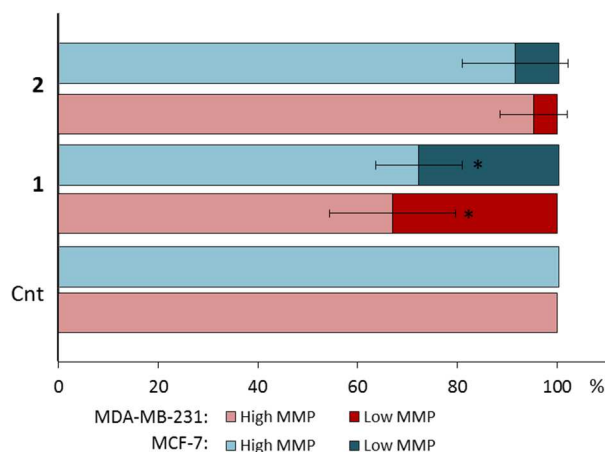


Figure 7. MCF-7 and MDA-MB-231 cells, treated with **1** and **2** (40 μM , 18 h) were evaluated for MMP, using TMRM probe. The percentage of cells with low and high MMP was depicted (* $p < 0.05$).

Lipid peroxidation in MDA-MB-231 cells after treatment with **1** or **2**

To get further insight into the mechanism of action of **1** and **2**, we have tested their ability to induce lipid peroxidation on MDA-MB-231 cells. Lipid peroxidation results from the attack of (poly)unsaturated lipids by reactive oxygen species (ROS) and is representative of oxidative stress. The level of malondialdehyde (MDA) as end-product of lipid peroxidation was evaluated by a fluorimetric assay. Of note, the results showed that **1** is able to induce a net increase of MDA of 20-30% in a concentration-dependent fashion while **2** has no effect (Figure 8).

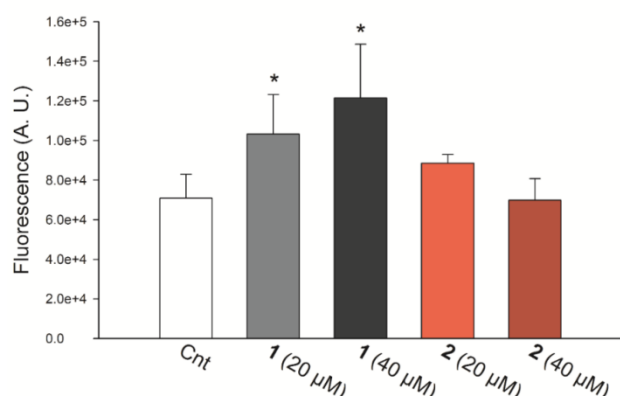


Figure 8. Lipid peroxidation induced by **1** and **2** in MDA-MB-231 cells. The colored adduct was evaluated with a fluorimetric assay at 530 nm (Ex) and 590 nm (Em) (see Experimental Section for details). (* $p < 0.05$)

Comparison of the amount of iron in cells incubated with **1** or **2**

Iron was quantified by ICP-OES (Inductively Coupled Plasma Optical Emission Spectroscopy) in MDA-MB-231 and MCF-7 cell lysates after incubation in the presence of 40 μM **1** or **2** for 18 h.

The results (Table 2) show that the amount of iron found in MCF-7 and MDA-MB-231 cells incubated with **1** is significantly higher than with compound **2** (1:2 ratio around 2.5). After subtraction of endogenous iron contribution, the ratio between the amount of **1** and **2** in whole cells raises to 2.9 in MCF-7 and 6.1 in MDA-MB-231. This difference cannot be explained by a different lipophilicity between the two complexes (Log Po/w = 5.0 for **1**, 4.4 for **2**),^{25, 38} but could be related to their difference in cytotoxicity. Indeed, after incubation for 18 h, it is expected that the cytotoxic complex **1** has reacted with specific targets (proteins, DNA, etc.), resulting in its sequestration within cells. By contrast, the less cytotoxic compound **2** has less reacted, allowing its partial but significant release from the cells.

Table 2. Amount of iron (ng/mg protein) quantified by ICP-OES in MCF-7 and MDA-MB-231 cells incubated with **1** or **2** (40 μM) for 18 h.^[a]

	MCF-7	MDA-MB-231
Control cells	120 \pm 36	110 \pm 50
1	1070 \pm 245	691 \pm 90
2	527 \pm 150	298 \pm 42

^[a] mean of two experiments \pm SD

Quantification of iron in individual cell compartments

MDA-MB-231 and MCF-7 cells were incubated with 40 μM of **1** for 18 h. Cells were collected and fractionated into crude nuclear, mitochondrial and cytosolic fractions. Iron was quantified in each of these compartments by ICP-OES (Table 3 and Figure S7).

Table 3. Subcellular distribution (%) of iron measured by ICP-OES in MCF-7 or MDA-MB-231 cells incubated with 40 μM of **1** for 18 h.

	Cytosolic fraction (%)	Mitochondrial fraction (%)	Crude nuclear fraction (%)
MCF-7 ^[a]	14	35	51
MDA-MB-231 ^[b]	10.8 \pm 0.4	25 \pm 1.6	64.2 \pm 1.3

^[a] one experiment ; ^[b] mean of 2 experiments

The majority of the iron is located in the crude nuclear fraction. It is slightly higher for MDA-MB-231 cells than for MCF-7 (64.2% vs. 51%). The amount of endogenous iron in this fraction is negligible (ca. 8 - 10%). The second largest concentration of iron was found in mitochondria, where it was slightly higher for MCF-7 than for MDA-MB-231 (35% vs. 25%). Once again, the contribution of endogenous iron is negligible (ca. 10%). Finally, the amount of iron found in cytosol is low whatever the cell line with the proportion of endogenous iron ranging from 25 - 42% according to the cell line (Figure S7).

Discussion

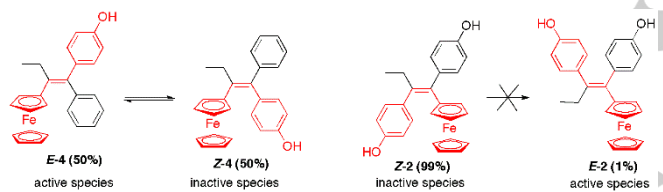
The results obtained with **1** and **2**, not only allow a better understanding of their own mechanisms of action, but also explain the difference in their cytotoxicity.

The unique feature common to complexes **1** and **2** is their powerful inhibition of TrxR *in vitro* after enzymatic oxidation by the HRP/H₂O₂ system (IC₅₀ around 30 nM). Furthermore, they both interact with its cysteine and selenocysteine residues. This activity is in accord with the fact that in both cases enzymatic oxidation leads to the formation of a quinone methide that can

undergo a 1,8-Michael addition with the Cys and Sec residues of TrxR. In MDA-MB-231 cells, complex **1** induces only weak inhibition of TrxR and no inhibition in Jurkat cells. This result suggests that inhibition of TrxR is not a critical factor in the cytotoxicity of **1**.

In terms of differences, we note that enzymatic oxidation of **1** by the HRP/H₂O₂ mixture involves the ferrocenyl moiety and contrasts with that of its organic analogue **6**; moreover, oxidation of **2** does not proceed via initial reaction at iron but instead parallels that found for the organic compound **7**. This difference appears to be crucial since the oxidation of Fe (II) to Fe (III), which constitutes the first step of the activation of **1** (and **3**) and is accompanied by the production of ROS in variable amounts,^{39, 40} is not observed with **2**.¹⁷ It is confirmed here by the effect on lipid peroxidation observed for **1**, and not for **2**. This process may be associated with the production of ROS, which seemingly play an important role in the cytotoxicity of **1**. Indeed, on MCF-7 cells, co-incubation of **1** with N-acetyl cysteine, a known antioxidant, acting as a ROS scavenger, resulted in the loss of its cytotoxic activity (Figure S8).

We have previously demonstrated that the cytotoxicity of ferrocifens is associated with their unique redox properties and the presence of a ferrocenyl / double bond / phenol motif.^{14, 17} In the monophenolic complex **4**, or the diphenolic complex **2**, the ferrocenyl and phenol substituents may in principle adopt either the *trans* (*E*-**4**, *E*-**2**) or *cis* (*Z*-**4**, *Z*-**2**) structures (Scheme 5); however, as noted above, **2** is found only as the *Z*-**2** isomer.



Scheme 5. Consequences of the E/Z isomerization of **4** and of the failure of **2** to undergo E/Z isomerization.

It therefore seems plausible to hypothesize that only the *trans* form of the complexes that exists for **4** and for **1**, but not for **2**, facilitates the oxidation of Fe (II) to Fe (III), with consequent production of ROS in the cell. This hypothesis also explains the two-fold cytotoxicity difference between **1** and **4** (0.6 and 1.13 μ M)³⁴.

Because of the approximately equal distribution of the *cis* and *trans* forms of the monophenol **4**, only 50% of the active *E* form is initially present in solution; of course, in the case of the diphenol **1** every molecule possesses a phenol substituent *trans* to the ferrocenyl moiety. This assumption is in accordance with the observation that all quinone methides obtained by chemical oxidation of ferrocifens that are sufficiently stable to have been characterized unequivocally are found only as the *E* isomer. This was initially confirmed by the X-ray crystal structure of a QM stabilized by the incorporation of two methyl substituents ortho to the carbonyl group,¹³ and by another very recent study in which several QMs stabilized by an atypical lone pair- π interaction have also been structurally characterized.⁴¹

This result may be explained as follows: let us consider the mechanism of the stepwise oxidation process to form the QM, as shown in Scheme S1. To allow delocalization of the initially formed radical cation from the ferrocenyl to the hydroxy

substituent on the phenol, and subsequently from the QM back to the carbon adjacent to the ferrocenyl, the connecting framework must be almost planar to have favourable orbital overlap through the π system. This is ideal in the *E*-isomer but would be impossible in the *Z* case since coplanarity of the C₆H₅ ring of the ferrocenyl unit and the *cis*-disposed QM ring would engender serious steric problems.

In summary, the lower cytotoxicity of **2**, can be explained by the fact that the *Z* configuration of complex **2** does not allow expression of the singular redox effects of ferrocene, which are observed only when the sequence is concatenated as: *trans* ferrocene / double bond / phenol. Molecule **2** can indeed suffer oxidation but, in this case, its initial behaviour parallels that of its organic counterpart by forming a diquinone, **9**, rather than exhibiting the redox effect of ferrocene, which is at the origin of the cytotoxicity of **1**.

The results obtained also make it possible to compare the mechanism of action of **1** with that of the tamoxifen-like complex, **3** (Figure 1); in particular, they highlight two essential differences. First of all, **1** scarcely inhibits thioredoxin reductase activity in Jurkat cells (Figure S6) whereas **3** inhibits it significantly (100% of inhibition with 15 μ M of **3**)²⁸ this behaviour is attributed to the cyclization, in cells, of the quinone methide **8** to form the corresponding indene **14** (Scheme 4).²⁶ Secondly, **1** does not induce MMP variation in Jurkat cells; this indicates the non-involvement of mitochondria in the cytotoxicity of **1**, in contrast to **3**,²⁸ thus confirming the essential role played, in this interaction, by the dimethylaminopropyl chain which confers on **3** the character of a lipophilic cation.²⁸ Given this observation, the result of the quantification of iron in different cellular compartments (mitochondria, crude nuclear extract, cytosol) may be surprising. In fact, a significant percentage of the iron is found in the mitochondria of the cells incubated with **1** (35% in MCF-7 cells, 25% in MDA-MB-231 cells, Table 3), even though the product does not have an effect at this level. This confirms the fact, previously observed, that the places where one finds the high concentrations of complexes are not necessarily those where they exert their effect, but are rather related to their lipophilicity.^{42, 43} The quantities of iron found are also very similar to those obtained for **4** in Jurkat cells (37% in mitochondria of Jurkat cells),³¹ a complex whose lipophilicity is close to that of **1** (Log Po/w around 4.5).

Conclusions

In conclusion, comparisons of the reactivity and the biological behaviour of diphenols **1** and **2** make it possible to better understand their mechanisms of action by highlighting the importance of the *trans* configuration in the “ferrocenyl / double bond / phenol” sequence in expressing the cytotoxicity of ferrocifens. It also confirms that, even though **1** and **3** have very similar cytotoxicities on MDA-MB-231 cells, their mechanism of action differs in some respects. Indeed, in addition to the limited inhibition of TrxR in the cells, we report here that **1** has only a slight effect on mitochondria. This leads to the idea that its mechanism of action is essentially associated with a redox imbalance, as demonstrated by lipid peroxidation and thiol oxidation, whereas that of **3** implies in addition an effect on mitochondria. Eventually, comparison of the biological behaviour of the highly cytotoxic complex **1**, with that of the poorly cytotoxic complex **2**, let us move forward in the understanding of the mechanism of action of **1**, one hit in the ferrocifen series.

Experimental Section

Materials

Compounds **1** and **2** were synthesized according to literature procedures.^{19, 25} Stock solutions (10 mM) were prepared in DMSO.

Enzymatic oxidation with the mixture HRP/H₂O₂

Enzymatic oxidation of the compounds (25 - 50 μ M) by HRP (46 nM) and H₂O₂ (200 μ M) was performed at pH 8.1 in buffer (0.2 M Tris-HCl, 1 mM EDTA) containing 10% DMSO. HRP (40 μ l of 1.14 μ M solution) and H₂O₂ (20 μ l of 10 mM solution) were pre-incubated for 5 min and then added to the solution of the compounds (940 μ l). The solution was immediately transferred to a cuvette and the UV-Visible spectrum was recorded between 250 and 650 or 750 nm on a Cary 50 spectrometer (Varian, Palo Alto, CA, USA). Rate constant k_{obs} of oxidation of **1** was calculated by fitting OD_{560nm}, versus time data according to the first order law equation (1) with Kaleidagraph software.

$$(1) \text{ OD} = C_0 + C_1 \times \exp(-k_{\text{obs}} \times t)$$

TrxR1 activity *in vitro*

Thioredoxin reductase activity was determined by estimating the DTNB reducing property of TrxR1 in the presence of NADPH. Aliquots of highly purified TrxR1 in 0.2 M Tris-HCl buffer (pH 8.1), 1 mM EDTA and 0.25 mM NADPH were preincubated for 5 min with the compounds. Afterwards, the reaction was initiated with 1 mM DTNB and monitored spectrophotometrically at 412 nm for about 10 min. For the formation of oxidized ferrociphenol derivatives of **1** and **2**, freshly prepared compounds, at increasing concentrations, were incubated for 15 min in 0.2 M Tris-HCl buffer (pH 8.1) containing 1 mM EDTA, 0.1 mM H₂O₂ and 22 nM HRP. Then, TrxR1 and 0.25 mM NADPH were added and incubated for another 5 min. Finally, the reaction was initiated with 1 mM DTNB and monitored spectrophotometrically at 412 nm for about 10 min.

BIAM assay

Compounds **1** and **2** (4 μ M) were treated with the mixture of 22 nM HRP/0.1 mM H₂O₂ for 15 min. Then, TrxR1 (1 μ M) pre-reduced with 60 μ M NADPH, was incubated for 30 min with 2 μ M of the compounds and of their derivatives, in 50 mM Tris-HCl buffer (pH 7.4) containing 200 μ M NADPH and 1 mM EDTA. After incubation, 8 μ L of the reaction mixture were added to 8 μ L of 100 mM biotinylated iodoacetamide (BIAM) in 0.1 M Tris-HCl at pH 8.5 or in 0.1 M HEPES-Tris at pH 6.0. Samples were incubated at room temperature (rT) for additional 30 min to allow BIAM alkylation of free -SH/SeH groups of the enzyme. Then, BIAM-modified enzyme was subjected to SDS-PAGE (10% gel), and transferred to a nitrocellulose membrane. BIAM labelled enzyme was detected with HRP conjugated streptavidin and enhanced chemiluminescence detection.

MTT proliferation assay

Cells (5 \times 10³) were seeded in a 96-well plate and treated with the compounds dissolved in DMSO. After 72 h, the medium was removed and 100 μ L of MTT solution (0.5 mg/mL) in PBS 1X were added. After 3 h in the dark at 37° C and 5% CO₂, the MTT solution was gently removed and the reaction was stopped with 100 μ L of 90% isopropanol and 10% dimethyl sulfoxide. Then, the absorbance was recorded (Abs₅₉₅₋₆₉₀) using a Tecan plate reader (Tecan Infinite® M200 PRO, Männedorf, CH).

TrxR and GR activities in cell lysates

Cells (1 \times 10⁶) were incubated for 18 h in the presence of the compounds and then harvested and washed with PBS. Each sample was lysed with a modified RIPA buffer: 150 mM NaCl, 50 mM Tris-HCl, 1 mM EDTA, 1% Triton X-100, 0.1% SDS, 0.5% DOC, 1 mM NaF and an antiprotease

cocktail ("Complete" Roche, Mannheim, Germany) containing 0.1 mM PMSF. After 40 min at 4 °C, the lysates were centrifuged at 12000g, to discard the debris, and tested for total TrxR activity. The reaction was started by the addition of 0.1 M DTNB (5,5'-dithiobis(2-nitrobenzoic acid)). The absorbance of the DTNB reduction product was followed at 412 nm at 25 °C. Glutathione reductase activity of cell lysates was measured in 0.2 M Tris-HCl buffer (pH 8.1), 1 mM EDTA, and 0.25 mM NADPH. The assay was initiated by addition of 1 mM GSSG and followed spectrophotometrically at 340 nm.

Total thiol assay

MDA-MB-231 and MCF-7 cells (3.5 \times 10⁵) were seeded in a 6-well plate and treated with the compounds. After 18 hours, the plate was washed with 1 mL PBS 1X. Cells were then dissolved with 1 mL of 0.2 M Tris/HCl (pH 8.1), 5 mM EDTA and 7.2 M guanidine. Reaction was started by the addition of 0.1 M DTNB. The absorbance of DTNB reduction product was followed at 412 nm at 25 °C.

Mitochondrial membrane potential assay

Cells (1 \times 10⁶) were seeded in a 25 cm² flask and then treated with the compounds for 18 h. Subsequently, the cells were washed with PBS 1X and 10 mM glucose, trypsinized and centrifuged at 500g for 5 min. Afterwards, cells (2.5 \times 10⁵ per tube) were resuspended in PBS 1X and 10 mM glucose and incubated with 25 nM fluorescent probe tetramethyl rhodamine methyl ester (TMRM) (Thermo Fisher Scientific, Waltham, MA, USA), for 20 min. FACS analysis for TMRM was performed on FACSCanto™ II flow cytometer (Becton-Dickinson, Franklin Lakes, NJ, USA)

Lipid peroxidation assay

Cells (1 \times 10⁶) were treated with different concentrations of the compounds, for 18 h. After, cells were washed with PBS and disrupted with 1 mL of 50 mM H₂SO₄ and 150 μ L of 10% phosphotungstic acid (PTA) for 10 min at rT. Then, cells were scraped and centrifuged at 15600g for 10 min at 4° C. The obtained pellets were washed with 1 mL of 50 mM H₂SO₄ and 150 μ L of 10% PTA. Samples were kept at rT for 5 min and centrifuged again at 15600g for 10 min at 4°C. Afterwards, the pellets were dissolved with 350 μ L of 0.25% NONIDET P-40, 0.01% butylhydroxytoluene and 0.17% thiobarbituric acid and incubated at 95° C for 60 min. Samples, were ice-cooled for 5 min and centrifuged at 15600g for 10 min. The supernatants were added with 400 μ L of *n*-butanol, vigorously mixed and centrifuged at 15600g for 15 min. The fluorescence of the upper phase was analysed (Ex= 530 nm, Em= 590 nm) using a Tecan Infinite M200 PRO plate reader (Tecan Infinite® M200 PRO, Männedorf, CH). The discarded pellets were solubilized and subjected to protein determination.

Preparation of cellular sub-fractions

Cells were sub-fractionated essentially following the protocol already described.²⁸ Briefly, cells (3 \times 10⁷) were collected, washed with PBS and subjected to hypo-osmotic treatment with 2 mL of 10 mM NaCl, 1.5 mM MgCl₂, 10 mM Tris-HCl buffer (pH 7.5) for 5 min and gently homogenized using a Dounce tissue grinder. Afterwards, 1.4 mL of 525 mM mannitol, 175 mM sucrose, 2.5 mM EDTA, 12.5 mM Tris-HCl buffer (pH 7.5) were rapidly added. The homogenate was diluted to a final volume of 5 mL with 210 mM mannitol, 70 mM sucrose, 1 mM EDTA, 5 mM Tris-HCl buffer (pH 7.5) and subjected to differential centrifugation. The first step was carried out at 1300g for 5 min at 4° C to discard nuclei and non-disrupted cells. The mitochondrial fraction was pulled down from the supernatant at 15800g for 15 min at 4° C and washed twice. The crude soluble supernatant obtained from the mitochondrial isolation step was further centrifuged at 105000g for 15 min at 4° C to obtain the cytosolic fraction. Mitochondrial fractions were lysed using a modified RIPA buffer containing 50 mM Tris-HCl (pH 7.4), 150 mM NaCl, 1 mM EDTA, 1%

Triton X100, 0.1% SDS, 0.5% DOC, 1 mM NaF, supplemented with an antiprotease cocktail and 0.1 mM PMSF and subjected to protein determination with the Lowry assay.⁴⁴ The presence of cytochrome oxidase and Cyt c as mitochondrial markers was assessed by Western blot analysis in the mitochondrial fraction.

Iron assay by ICP-OES

Cells incubated for 18 h in the presence of 40 μ M of the compounds were collected as cell lysates (starting from 1×10^6 cells) or subjected to cell fractionation (starting from 24×10^6 cells) as reported in a previous paragraph. Cell lysates, mitochondria and crude nuclei fractions were dissolved in concentrated nitric acid (70%, ACS grade, 0.286 mL) and digested at 60 °C in an ultrasound bath for 1 h. Then the samples volume was brought to 10 mL by addition of water (final concentration of HNO₃ in the sample = 2%). The cytosol samples were adjusted to 2% HNO₃ by addition of proper volumes of HNO₃ and water (final volume = 10 mL Milli-Q grade water) and kept at 4° C for 48 h. Samples were clarified by quick centrifugation at 2600g for 5 min and filtered on 0.22 μ m PES membrane. Quantification of iron was performed at 238.204 nm using an Agilent 5100 instrument (Santa Clara, CA, USA). Iron standards were prepared from 1000 ppm stock solution (Fluka). The concentrations used for calibration were 0, 7.8, 15.6, 31.2, 62.5, 125, 250 and 500 ppb. Measurements were done in triplicate in two or three sets of independent experiments. ICP/OES experiments were performed on an Agilent 5100 SVDV at the ALIPP6 laboratory (ISTeP, Sorbonne Université)

Acknowledgements

M.P.R. and V.S. acknowledge BIRD187299/18 granted by University of Padova (Italy); the Authors thank Sébastien Blanchard (IPCM, Sorbonne Université) for EPR measurements.

Keywords: Bioorganometallic chemistry; cancer; iron; lipid peroxidation; thioredoxin reductase

References

- N.P.E. Barry and P.J. Sadler, *Chem. Commun.*, **2013**, 49, 5106-31.
- G. Gasser, I. Ott, and N. Metzler-Nolte, *J. Med. Chem.*, **2011**, 54, 3-25.
- E. Wong and C.M. Giandomenico, *Chem. Rev.*, **1999**, 99, 2451-66.
- C.G. Hartinger and P.J. Dyson, *Chem. Soc. Rev.*, **2009**, 38, 391-401.
- P.Y. Zhang and P.J. Sadler, *J. Organomet. Chem.*, **2017**, 839, 5-14.
- B. Albada and N. Metzler-Nolte, *Chem. Rev.*, **2016**, 116, 11797-839.
- S.M. Meier-Menches, C. Gerner, W. Berger, C.G. Hartinger, and B.K. Keppler, *Chem. Soc. Rev.*, **2018**, 47, 909-28.
- E.A. Hillard, A. Vessières, and G. Jaouen, *Ferrocene Functionalized Endocrine Modulators as Anticancer Agents*, in *Top Organometal Chem.* 2010. p. 81-117.
- G. Jaouen and S. Top, *The ferrocifen family as potent and selective antitumor compounds: mechanisms of action*, in *Advances in Organometallic Chemistry and Catalysis*, A.J.L. Pombeiro, Editor. 2014, Wiley. p. 561-80.
- G. Jaouen, A. Vessières, and S. Top, *Chem. Soc. Rev.*, **2015**, 44, 8802-17.
- A. Vessières, *J. Organomet. Chem.*, **2013**, 734, 3-16.
- A. Vessières, *Iron Compounds as Anticancer Agents*, in *Metal-based Anticancer Agents*, A. Casini, A. Vessières, and S.M. Meier-Menches, Editors. 2019, Royal Society of Chemistry: Cambridge (UK). p. 62-90.
- D. Hamels, P.M. Dansette, E.A. Hillard, S. Top, A. Vessières, P. Herson, G. Jaouen, and D. Mansuy, *Angew Chem Int Ed*, **2009**, 48, 9124-26.
- P. Messina, E. Labbé, O. Buriez, E.A. Hillard, A. Vessières, D. Hamels, S. Top, G. Jaouen, Y.M. Frapart, D. Mansuy, and C. Amatore, *Chem Eur J*, **2012**, 18, 6581-87.
- Y. Wang, M.A. Richard, S. Top, P.M. Dansette, P. Pigeon, A. Vessières, D. Mansuy, and G. Jaouen, *Angew Chem Int Ed*, **2016**, 55, 10431-34.
- Y. Wang, P.M. Dansette, P. Pigeon, S. Top, M.J. McGlinchey, D. Mansuy, and G. Jaouen, *Chem. Sci.*, **2018**, 9, 70-78.
- E.A. Hillard, A. Vessières, L. Thouin, G. Jaouen, and C. Amatore, *Angew. Chem. Int. Ed.*, **2006**, 45, 285-90.
- G. Jaouen, S. Top, A. Vessières, G. Leclercq, J. Quivy, L. Jin, and A. Croisy, *C. R. Acad. Sci. Paris*, **2000**, Série IIc, 89-93.
- S. Top, A. Vessières, G. Leclercq, J. Quivy, J. Tang, J. Vaissermann, M. Huché, and G. Jaouen, *Chem. Eur. J.*, **2003**, 9, 5223-36.
- M. Görmén, P. Pigeon, S. Top, E.A. Hillard, M. Huché, C.G. Hartinger, F. de Montigny, M.-A. Plamont, A. Vessières, and G. Jaouen, *ChemMedChem*, **2010**, 5, 2039-50.
- E. Allard, C. Passirani, E. Garcion, P. Pigeon, A. Vessières, G. Jaouen, and J.P. Benoit, *J. Control. Release*, **2008**, 130, 146-53.
- C. Bruyère, V. Mathieu, A. Vessières, P. Pigeon, S. Top, G. Jaouen, and R. Kiss, *J. Inorg. Biochem.*, **2014**, 141, 144-51.
- Q. Michard, G. Jaouen, A. Vessières, and B.A. Bernard, *J Inorg Biochem*, **2008**, 102, 1980-5.
- Y.L.K. Tan, P. Pigeon, E.A. Hillard, S. Top, M.-A. Plamont, A. Vessières, M.J. McGlinchey, H. Mueller-Bunz, and G. Jaouen, *Dalton Trans.*, **2009**, 10871-81.
- A. Vessières, S. Top, P. Pigeon, E.A. Hillard, L. Boubeker, D. Spera, and G. Jaouen, *J. Med. Chem.*, **2005**, 48, 3937-40.
- A. Citta, A. Folda, A. Bindoli, P. Pascal Pigeon, S. Top, A. Vessières, M. Salmain, G. Jaouen, and M.P. Rigobello, *J. Med. Chem.*, **2014**, 57, 8849-59.
- V. Scalcon, A. Bindoli, and M.P. Rigobello, *Free Radic Biol Med*, **2018**, 127, 62-79.
- V. Scalcon, M. Salmain, A. Folda, S. Top, P. Pigeon, H.Z.S. Lee, G. Jaouen, A. Bindoli, A. Vessières, and M.P. Rigobello, *Metallomics*, **2017**, 9, 949-59.
- O. Karaca, V. Scalcon, S.M. Meier-Menches, R. Bonsignore, J.M.J.L. Brouwer, F. Tonolo, A. Folda, M.P. Rigobello, F.E. Kuhn, and A. Casini, *Inorg Chem*, **2017**, 56, 14237-50.
- E. Schuh, C. Pfluger, A. Citta, A. Folda, M.P. Rigobello, A. Bindoli, A. Casini, and F. Mohr, *J Med Chem*, **2012**, 55, 5518-28.
- V.W. Winkler, M.A. Nyman, and R.S. Egan, *Steroids*, **1971**, 17, 197.
- Y. Ortin, J. Grealis, C. Scully, H. Muller-Bunz, A.R. Manning, and M.J. McGlinchey, *J. Organomet. Chem.*, **2004**, 689, 4683-90.
- V. Scalcon, A. Citta, A. Folda, A. Bindoli, M. Salmain, I. Ciofini, S. Blanchard, J.D. Cazares-Marinero, Y. Wang, P. Pigeon, G. Jaouen, A. Vessières, and M.P. Rigobello, *J. Inorg. Biochem.*, **2016**, 165, 146-51.
- H.Z.S. Lee, O. Buriez, F. Chau, E. Labbé, R. Ganguly, C. Amatore, G. Jaouen, A. Vessières, W.K. Leong, and S. Top, *Eur. J. Inorg. Chem.*, **2015**, 4217 - 25.
- G.H. Degen and J.A. McLachlan, *Chem. Biol. Interac.*, **1985**, 54, 363-75.
- V. Scalcon, S. Top, H.Z.S. Lee, A. Citta, A. Folda, A. Bindoli, W.K. Leong, M. Salmain, A. Vessières, G. Jaouen, and M.P. Rigobello, *J Inorg Biochem*, **2016**, 160, 296-304.
- M.-A. Richard, D. Hamels, P. Pigeon, S. Top, P.M. Dansette, H.Z.S. Lee, A. Vessières, D. Mansuy, and G. Jaouen, *ChemMedChem*, **2015**, 10, 981-90.

38. E.A. Hillard, A. Vessières, S. Top, P. Pigeon, K. Kowalski, M. Huché, and G. Jaouen, *J. Organomet. Chem.*, **2007**, 692, 1315-26.
39. C. Lu, J.M. Heldt, M. Guille-Collignon, F. Lemaitre, G. Jaouen, A. Vessières, and C. Amatore, *ChemMedChem*, **2014**, 9, 1286-93.
40. A. Vessières, C. Corbet, J.M. Heldt, N. Lories, N. Jouy, I. Laios, G. Leclercq, G. Jaouen, and R.A. Toillon, *J Inorg Biochem*, **2010**, 104, 503-11.
41. Y. Wang, P. Pigeon, S. Top, J. Sanz Garcia, C. Troufflard, I. Ciofini, M.J. McGlinchey, and G. Jaouen, *Angew Chem Int Ed Engl*, **2019**, 58, 8421-25.
42. S. Clede, F. Lambert, C. Sandt, S. Kascakova, M. Unger, E. Harte, M.A. Plamont, R. Saint-Fort, A. Deniset-Besseau, Z. Gueroui, C. Hirschmugl, S. Lecomte, A. Dazzi, A. Vessières, and C. Policar, *Analyst*, **2013**, 138, 5627-38.
43. F. Fus, Y. Yang, H.Z.S. Lee, S. Top, M. Carriere, A. Bouron, A. Pacureauu, J.C. da Silva, M. Salmain, A. Vessières, P. Cloetens, G. Jaouen, and S. Bohic, *Angew Chem Int Ed Engl*, **2019**, 58, 3461-65.
44. O.H. Lowry, N.J. Rosebrough, A.L. Farr, and R.J. Randall, *J Biol Chem*, **1951**, 193, 265-75.